nature geoscience

SUPPLEMENTARY INFORMATION

DOI: 10.1038/NGEO1863

Imprint of Southern Ocean eddies on winds, clouds and rainfall

I. Frenger[1,2*], N. Gruber[1,2], R. Knutti[3] and M. Münnich[2]

[1]Center for Climate Systems Modeling (C2SM)

[2]Environmental Physics, Institute of Biogeochemistry and Pollutant Dynamics

[3]Climate Physics, Institute for Atmospheric and Climate Science

ETH Zürich, Universitätstrasse 16, 8092 Zürich, Switzerland

*ivy.frenger@env.ethz.ch

Supplementary Methods

Data

The altimeter product, i.e. sea level anomalies exploited for eddy identification are produced by Ssalto/Duacs and distributed by Aviso, with support from Cnes (version v3.0.0, available at `http://www.aviso.oceanobs.com/duacs/`). The AMSR-E and QuikSCAT data are produced by Remote Sensing Systems (available at `http://www.remss.com`) and sponsored by the NASA Ocean Vector Winds Science Team as well as the NASA Earth Science MEaSUREs DISCOVER Project and the AMSR-E Science Team. The cloud fraction data are processed and distributed by the ACRI-ST GlobColour service (available at `http://www.globcolour.info`), supported by EU FP7 MyOcean & ESA GlobColour Projects, using ESA ENVISAT MERIS data, NASA MODIS and SeaWiFS data.

Eddy Tracking

The eddies were tracked over time to be able to select eddies which were detected in at least two consecutive time steps (see Methods Section): to track an eddy, we determined the location of the matching eddy in the consecutive time step by first estimating its possible position taking into account the advection by the mean currents and the eddies' intrinsic phase speed, which is assumed to be close to the one of linear baroclinic Rossby waves [1]. We then drew a search ellipse around our projection of the eddy location considering the variability of currents and eddy behaviour. If we found more than one potentially matching eddy for e_1 within the search ellipse, for instance e_2 and e_3, we applied a similarity-criteria similar to studies before (e.g. [2]), i.e. selected the most similar eddy as matching

eddy: $\min(D_{e_1,e_{2,3}})$ with $D_{e_1,e_{2,3}} = \frac{1}{\sqrt{4}}\sqrt{\left(\frac{\Delta\omega}{\sigma_\omega}\right)^2 + \left(\frac{\Delta a}{\sigma_a}\right)^2 + \left(\frac{\Delta SST}{\sigma_{SST}}\right)^2 + \left(\frac{\Delta d}{d_{min}}\right)^2}$, and $\Delta\omega = |\omega_{e_1} - \omega_{e_{2,3}}|$, $\Delta SST = |SST_{e_1} - SST_{e_{2,3}}|$, $\Delta a = |a_{e_1} - a_{e_{2,3}}|$ and $\Delta d = |d_{min} - d_{e_{2,3}}|$, where a is the individual eddy amplitude, d_{min} the minimum of the spatial distances of all eddies located within the search ellipse from the projected location of e_1, SST the sea surface temperature and σ_ω, σ_a and σ_{SST}, i.e., the temporal standard deviations of ω, a and SST, are taken from maps of temporal standard deviations which we derived based on all identified (not yet tracked) eddies. We applied two final constraints concerning the match-up: firstly, we allowed a match only if $D_{e_1,e_{2,3}} < 1$ to exclude a match which would involve highly unlikely changes in eddy properties from e_1 to $e_{2,3}$. Secondly, we aimed to filter out "dying eddies" by not allowing an (5%) increase in vorticity if the eddy's vorticity had decreased the previous three time steps and also showed a 50% decease of vorticity compared to the time of first detection. In case that either no eddy centre was located within the search ellipse or all eddies within the search ellipse were rejected as matching eddies, e_1 was assumed to have died. We did not try to search for lost eddies in the following time steps.

Note about the mean composite eddy (Fig. 2 and Supplementary Fig. S5)

The variables were averaged in a rotated coordinate system according to the large-scale wind direction as one anticipates a different state of the atmosphere up- and downstream of the SST perturbation, and in addition a downwind shift of the perturbed atmosphere relative to the SST anomaly. The large-scale wind direction was defined as the average wind direction in a square of 14 eddy radii centred relative to the eddy-core. The SST anomaly and sea level anomaly contours are closely linked in the mean composite figure. A pronounced shift of the SST anomaly associated with oceanic eddies (relative to sea level anomalies contours) was detected in quiescent areas, whereas it is very small and not directly visible in dynamic areas, such as the Antarctic Circumpolar Current (ACC) [3]. If we distinguish eddies related to the ACC from the ones to the north, we find a clear dipole structure/shift of the SST anomaly and the sea level anomalies in the more quiescent region north of the ACC, too (not shown). However, in our domain, as the mean composite of eddies is dominated by eddies of dynamic areas which generally show a larger SST anomaly than eddies in quiescent regions, the dipole pattern due the shift has a much weaker amplitude [3]. Also, the feature of the SST and sea level anomaly shift is not directly relevant for the point of air-sea interaction we would like to make in this paper.

Supplementary Note S1: Scaling Argument Concerning the Impact of Oceanic Eddies on the Lower Atmosphere

The scaling argument entails two steps. First, we need to show that the overlying atmosphere responds quickly to anomalous surface fluxes associated with SST anomalies, and second, we need to demonstrate that the anomalous heat fluxes are of a magnitude large enough to modify the marine atmospheric boundary layer significantly. We first discuss the adjustment time-scale, and then provide a brief scaling estimate of the energy added to the atmospheric boundary layer due the effect of oceanic eddies.

Time-scale of adjustment

While air-sea fluxes will respond instantaneously to a disequilibrium, it will take time for the overlying atmosphere to adjust, and this time-scale has to be shorter than the time the air spends over the eddy and its associated SST anomalies. We estimate the latter to be about 4.5 to 5.5 hours, assuming an air-speed of 10 $^{m}/_{s}$ and an extent of 160 to 240 km of the eddy-induced SST anomalies (2 to 3 times larger than the pure eddy core). This is longer than the time-scale associated with the subsequent modification of the marine atmospheric boundary layer turbulence, i.e., about 1 hour, as estimated by [4] based on satellite observations and model simulations. Therefore, we can assume that the boundary layer above the SST anomalies will have sufficient time to adjust to them.

The tight spatial coupling between the SST and atmospheric anomalies with only a small downwind displacement further supports this conclusion. The somewhat larger displacements of cloud properties and rainfall compared to wind speed (at least for anticyclones), indicates that near surface wind responds quickest, whereas the responses of clouds and rainfall, which are related to processes at the top of the atmospheric boundary layer, are slightly delayed.

Our arguments are also consistent with what is known about the diurnal cycle of the atmospheric boundary layer over land (although clearly the magnitude of the forcing is much larger there). During the day, when the surface is being heated and the vertical momentum exchange increases, the near-surface wind speeds are higher − analogous to the increased wind over a positive SST anomaly. During the night, surface cooling stabilizes the atmospheric boundary layer and decreases the vertical momentum transport, i.e. turbulence. As a result, near-surface wind speeds tend to be very low and a nocturnal jet may develop aloft.

Energy flux scaling argument

For a typical warm-core eddy SST anomaly for Southern Ocean conditions of $\Delta\mathrm{SST} = 0.3\ ^{\circ}\mathrm{C}$ (mean over core and peripheral area), a standard bulk formula for surface fluxes provides an estimate of the additional heat flux into the atmospheric boundary layer of $\Delta Q = 20\ \mathrm{W\ m^{-2}}$

([5], 200 W m^{-2} for $\sim$ 3 °C). For an exposure time to this SST anomaly of $t = 4$ h and an atmospheric boundary layer height of $H = 500$ m this leads to a mean temperature change in the atmospheric boundary layer of $\Delta T = \Delta Q t/(H \rho_{\mathrm{air}} c_p) = 0.6$ °C (density of air ρ_{air} =1 kg m^{-3}, specific heat capacity of air c_p=10^3 J kg^{-1} K^{-1}). Finally, assuming a well mixed atmospheric boundary layer and a standard tropospheric lapse rate above of $\gamma = 6.5$ °C km^{-1}, we estimate an atmospheric boundary layer height change of $\Delta H \approx 100$ m or 20%, which is in the range of observations and modeling studies (e.g. [6, 7, 8]). Hence, the SST anomalies associated with ocean mesoscale eddies provide enough energy to cause measurable changes in the lower atmosphere despite their moderate size and the swiftly moving atmosphere.

Supplementary Figure S1

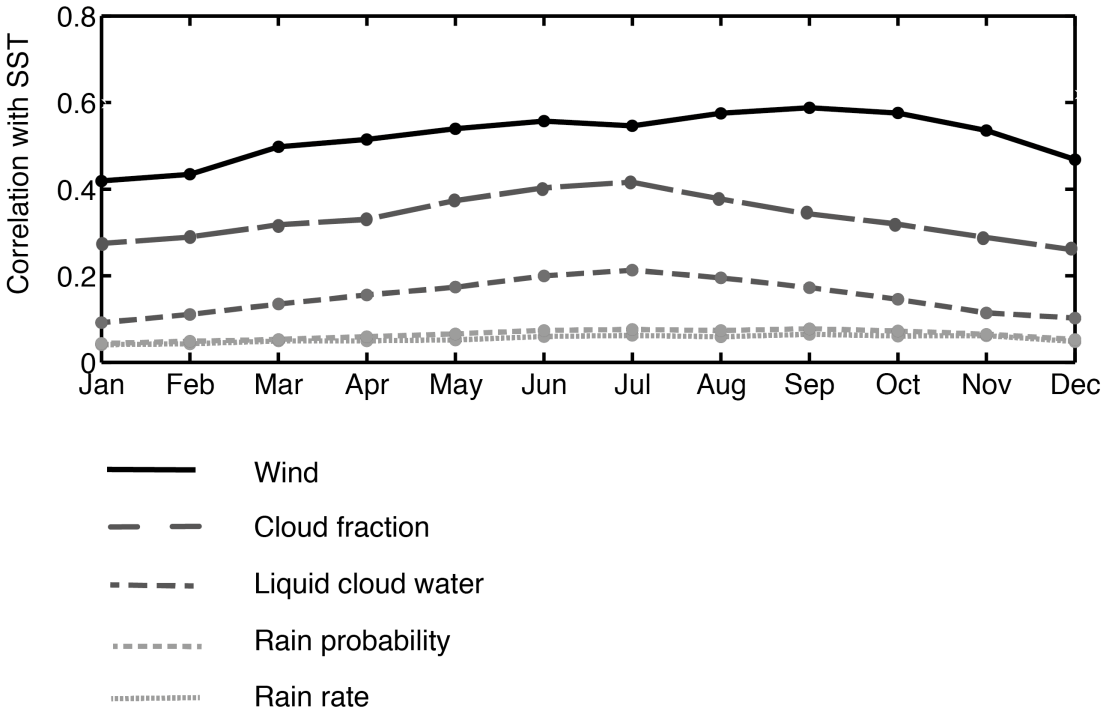

Figure S1: Seasonality of correlations of SST anomalies of oceanic eddies with anomalies of atmospheric properties (wind speed, cloud fraction, liquid cloud water, rain probability and rain rate); all eddies south of 30°S (>600,000) are considered in this Figure, i.e. several 10,000 data points contribute to the correlation for each month; correlations are significant for all months ($p<0.01$).

Supplementary Figure S2

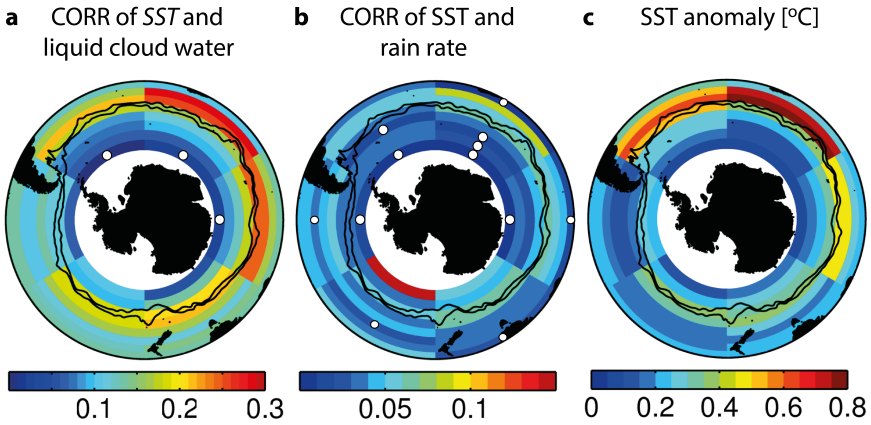

Figure S2: Polar orthographic maps of the eddy statistics (continued from Fig. 1). Correlations (CORR) in each 60°×4° bin of anomalies of SST of oceanic eddies with anomalies of **a** liquid cloud water and **b** rain rate; **c** shows the mean absolute SST anomaly in each bin. White dots mark bins in **a** and **b** where correlations are not significant ($p>0.01$) and white areas feature insufficient data; black contours denote the two major fronts of the Antarctic Circumpolar Current (the Subantarctic and the Polar Fronts).

Supplementary Figure S3

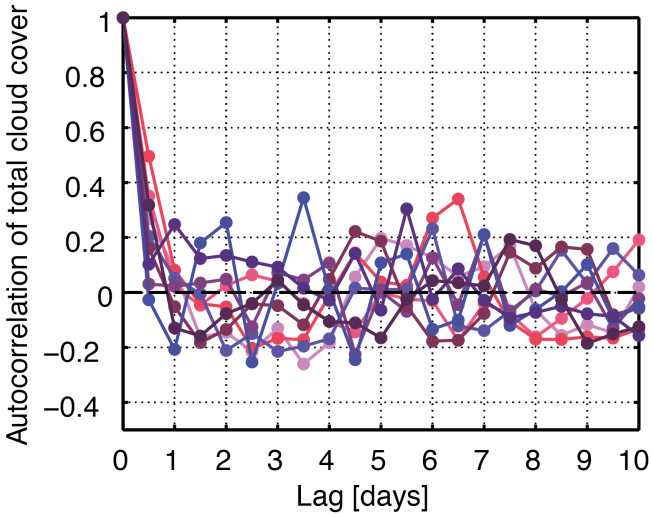

Figure S3: Autocorrelation of total cloud cover over various locations in the Southern Ocean (south of 30°S and north of 60°S at different latitudes over the Pacific, Atlantic and Indian Ocean) based on 12-hourly atmospheric reanalysis data (ERA-interim, `http://www.ecmwf.int/research/era/do/get/era-interim`) for a summer month, i.e., January 2008.

At all locations the autocorrelation of total cloud cover drops below 0.2 within 1 to 2 days (see Supplementary Fig. S3). The autocorrelations of other atmospheric quantities drop off similarly quickly (not shown). This confirms our expectation since atmospheric weather systems pass by quickly in the Southern Ocean, where there are no blocking situations over/next to land masses/topography that could induce longer persistence. Hence, we consider the weekly atmospheric data as statistically independent.

Supplementary Figure S4

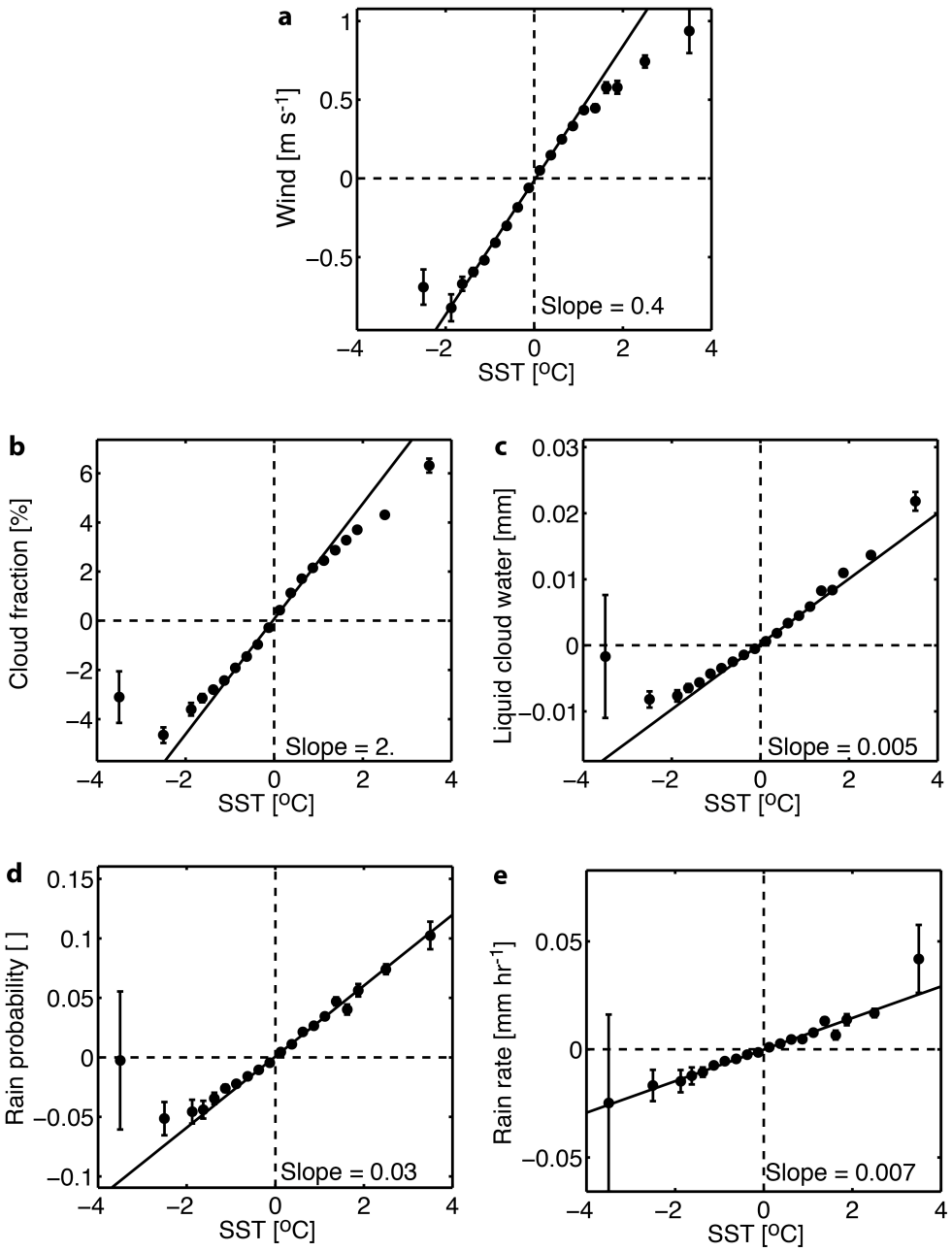

Figure S4: Linear relationship of SST anomalies of oceanic eddies and anomalies of atmospheric quantities. The atmospheric quantities, i.e. **a** wind speed, **b** cloud fraction, **c** liquid cloud water, **d** rain probability and **e** rain rate are binned according to the eddies' SST anomalies and averaged thereafter; the bin sizes are of 0.25°C and of 1°C spacing for anomalies smaller and larger than $|2°\mathrm{C}|$, respectively; the vertical bars show the error of the mean; the slope of the least square fit to the unbinned data shown as black line is noted in each panel; all eddies in the region south of 30°S (>600,000) are considered in this Figure.

The relationship of SST anomalies and atmospheric quantities is mostly linear with a change of wind of 0.4 m s^{-1}, of cloud fraction of 2%, of liquid cloud water of 0.005 mm, rain probability of 3% and rain rate of 0.007 mm h^{-1} per 1°C of SST anomaly; a robust fit (not shown) features the same slopes except for the rain rate where it is smaller (0.005 mm h^{-1}); the slope expressed relative to the background state is about 5% for wind, 3% for cloud fraction, 6% for liquid cloud water and 8% for both, rain rate and probability. The steepness of the slopes is relatively independent of the magnitude of the SST anomalies included in the regression and of the area, i.e. independent for instance of the Agulhas area with its large SST anomalies and high correlations. The steepness of the slopes increases with increasing large-scale wind speeds (not shown, in agreement with [8])
The slopes from our results agree well with previous findings of 0.2-0.4 m s^{-1} $°C^{-1}$ for wind speed over the Agulhas Return Current and the Malvinas-Brazil Confluence Zone [9, 10, 11]; further, absolute SST perturbations in the range of 1.5 to 3 °C in the Agulhas Return Current are associated with absolute liquid cloud water anomalies in the range of 0.01 to 0.02 mm [10] (Fig. 18 therein), matching approximately our results.

Supplementary Figure S5

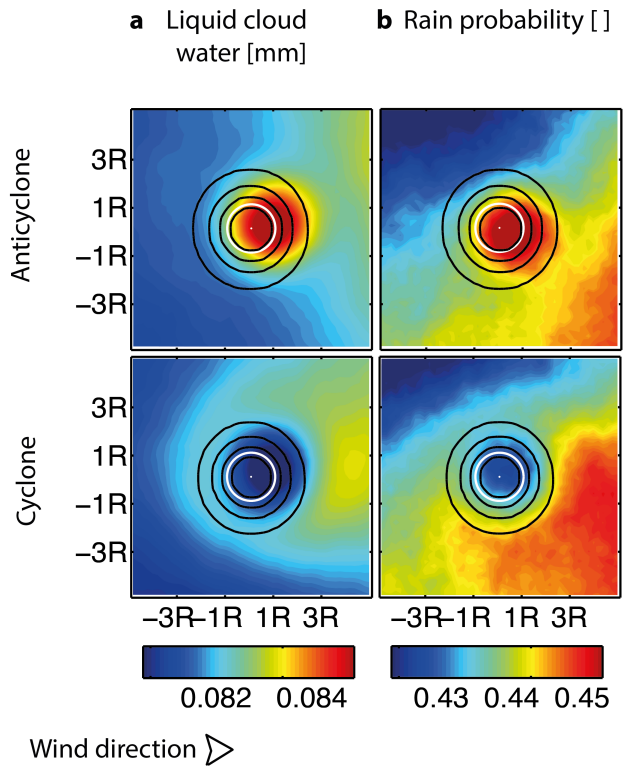

Figure S5: Mean eddy and and pattern of its atmospheric imprint (continued from Fig. 2). a Liquid cloud water ($\pm 0.3 \times 10^{-3}$ mm) and **b** rain probability ($\pm 3 \times 10^{-3}$); mean composite maps of the >600,000 individual eddy realizations south of 30°S, divided into anticyclones and cyclones; white circles mark the eddy-core as detected with the Okubo-Weiss parameter; black lines denote sea level anomaly contours associated with the eddy; before averaging, the eddies were scaled according to their individual eddy amplitude and radius (R), interpolated and rotated so that the large-scale wind is from left to right.

The large-scale gradient of SST is positive towards the equator (the wind direction is predominantly westerly); in contrast, the large-scale gradient is largely positive towards high latitudes for the atmospheric quantities, which reflects the increasing wind speed, cloud fraction and rain towards the "core-latitudes" of the westerlies.

A small downwind displacement is visible in the imprint of eddies on the atmosphere especially for the cloud properties and rain (see also Fig. 2 in the main text and Supplementary Note S1 about the response time-scale of the marine atmospheric boundary layer).

Supplementary Figure S6

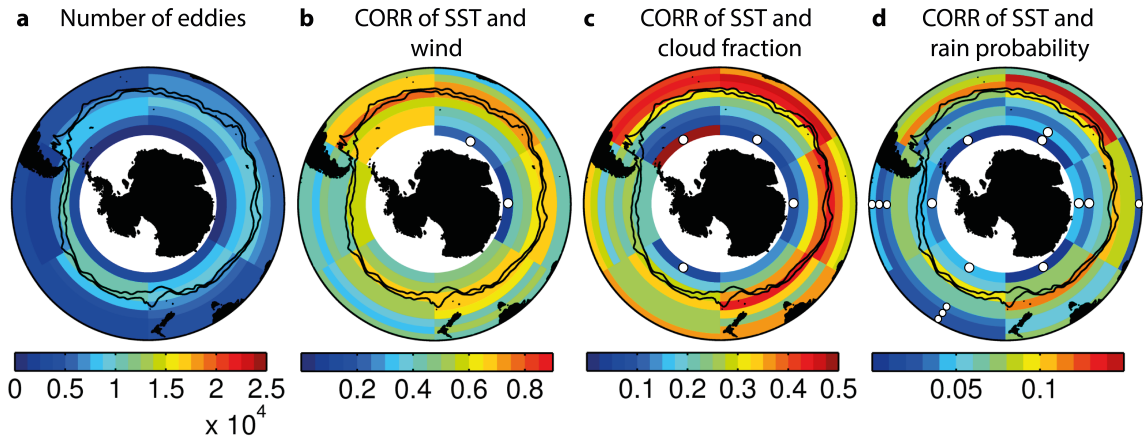

Figure S6: Polar orthographic maps of the eddy statistics: as Fig. 1 but with a reduced sample size (see Methods Section); only biweekly atmospheric data are considered and eddies with a minimum life time of 1 month.

Supplementary Figure S7

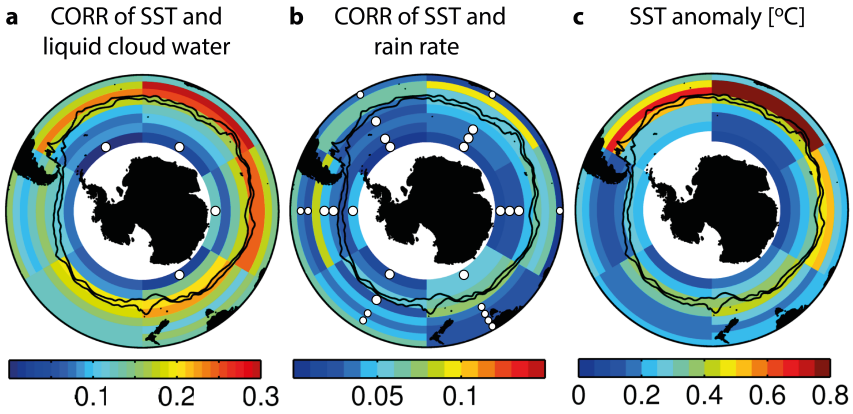

Figure S7: Polar orthographic maps of the eddy statistics: as Supplementary Fig. S2 but with a reduced sample size (see Methods Section); only biweekly atmospheric data are considered and eddies with a minimum life time of 1 month.

Supplementary Figure S8

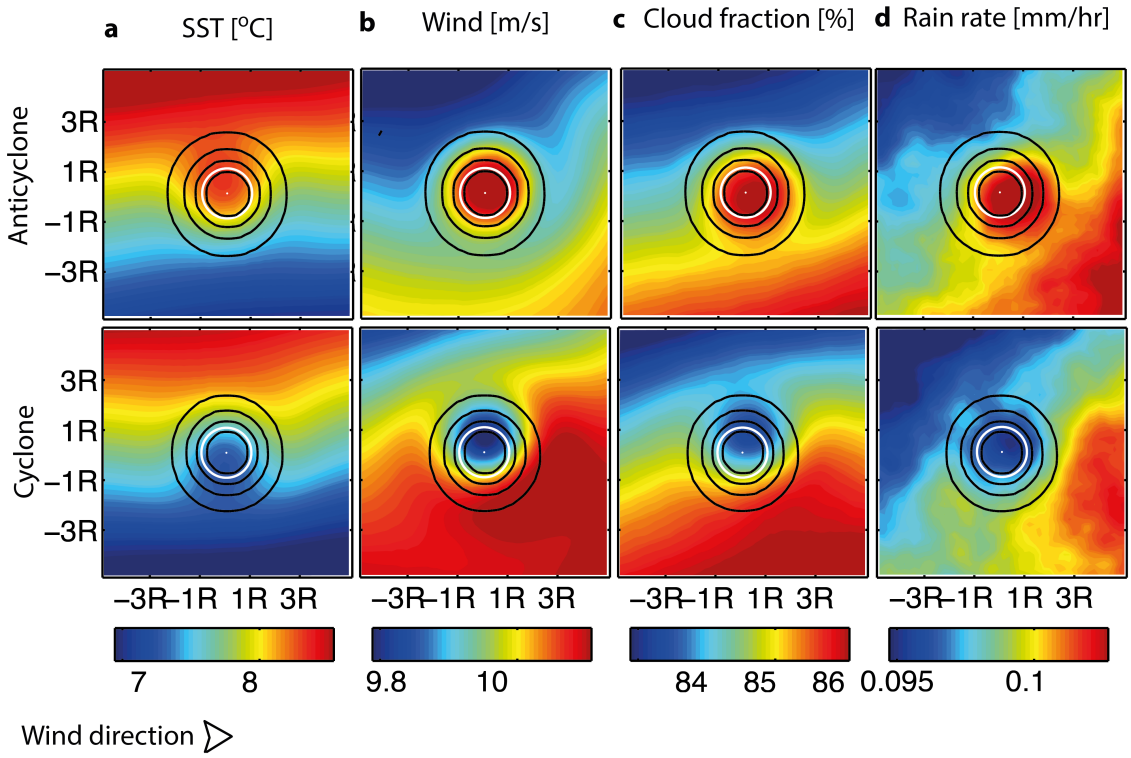

Figure S8: Mean eddy and and pattern of its atmospheric imprint: as Fig. 2 but with a reduced sample size (see Methods Section); only biweekly atmospheric data are considered and eddies with a minimum life time of 1 month.

Supplementary Figure S9

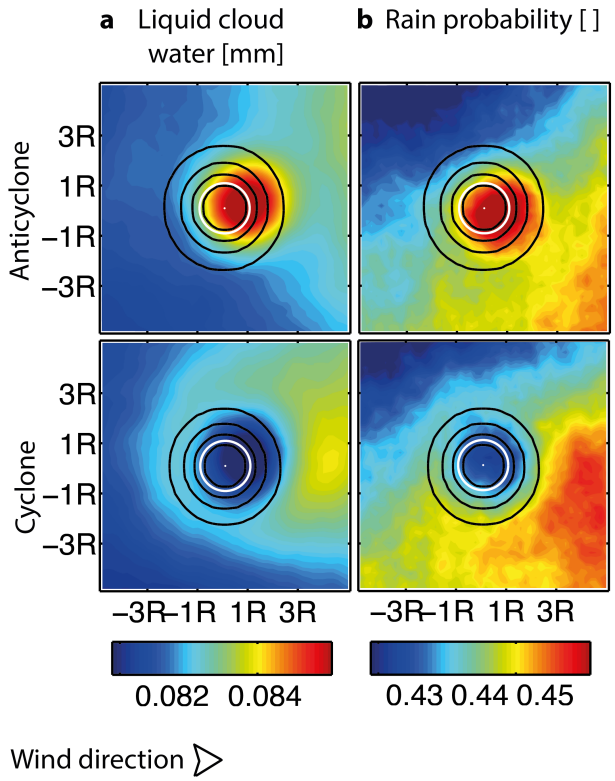

Figure S9: Mean eddy and and pattern of its atmospheric imprint: as Supplementary Fig. S5 but with a reduced sample size (see Methods Section); only biweekly atmospheric data are considered and eddies with a minimum life time of 1 month.

Supplementary Information References

[1] Chelton, D. B., DeSzoeke, R. A., Schlax, M. G., El Naggar, K. & Siwertz, N. Geographical variability of the first baroclinic Rossby radius of deformation. *Journal of Physical Oceanography* **28**, 433–460 (1998).

[2] Penven, P., Echevin, V., Pasapera, J., Colas, F. & Tam, J. Average circulation, seasonal cycle, and mesoscale dynamics of the Peru Current System: A modeling approach. *Journal of Geophysical Research* **110**, C10021, doi:10.1029/2005JC002945. (2005).

[3] Hausmann, U. & Czaja, A. The observed signature of mesoscale eddies in sea surface temperature and the associated heat transport. *Deep Sea Research Part I: Oceanographic Research Papers* **70**, 60–72 (2012).

[4] Park, K.-A., Cornillon, P. & Codiga, D. L. Modification of surface winds near ocean fronts: Effects of Gulf Stream rings on scatterometer (QuikSCAT, NSCAT) wind observations. *Journal of Geophysical Research* **111**, C03021, doi:10.1029/2005JC003016 (2006).

[5] Messager, C., Speich, S. & Key, E. Marine atmospheric boundary layer over some Southern Ocean fronts during the IPY BGH 2008 cruise. *Ocean Science* **8**, 1001–1023 (2012).

[6] Sweet, W. & Fett, R. Air-sea interaction effects in the lower troposphere across the north wall of the Gulf Stream. *Monthly Weather Review* **109**, 1042–1052 (1981).

[7] Kwon, B., Bénech, B. & Lambert, D. Structure of the marine atmospheric boundary layer over an oceanic thermal front: SEMAPHORE experiment. *Journal of Geophysical Research* **103**, 25159–25180, doi::10.1029/98JC02207 (1998).

[8] Spall, M. A. Midlatitude wind stress-sea surface temperature coupling in the vicinity of oceanic fronts. *Journal of Climate* **20**, 3785–3801 (2007).

[9] Liu, W. T., Xie, X. & Niiler, P. P. Ocean-atmosphere interaction over Agulhas extension meanders. *Journal of Climate* **20**, 5784–5797 (2007).

[10] O'Neill, L. W., Chelton, D. B., Esbensen, S. K. & Wentz, F. J. High-resolution satellite measurements of the atmospheric boundary layer response to SST variations along the Agulhas Return Current. *Journal of Climate* **18**, 2706–2723 (2005).

[11] O'Neill, L. W., Chelton, D. B. & Esbensen, S. K. Covariability of surface wind and stress responses to sea surface temperature fronts. *Journal of Climate* **25**, 5916–5942 (2012).